Diffusion Dominant Solute Transport Modelling In Deep Repository Under The Effect of Emplacement Media Degradation – 13285

S. Kwong[*] and A.P. Jivkov[**]

[*] National Nuclear Laboratory, UK, simon.kwong@nnl.co.uk.

[**] Research Centre for Radwaste and Decommissioning and Modelling and Simulation Centre, University of Manchester, UK.

ABSTRACT

Deep geologic disposal of high activity and long-lived radioactive waste is being actively considered and pursued in many countries, where low permeability geological formations are used to provide long term waste contaminant with minimum impact to the environment and risk to the biosphere. A multi-barrier approach that makes use of both engineered and natural barriers (i.e. geological formations) is often used to further enhance the containment performance of the repository.

As the deep repository system subjects to a variety of thermo-hydro-chemo-mechanical (THCM) effects over its long 'operational' lifespan (e.g. 0.1 to 1.0 million years, the integrity of the barrier system will decrease over time (e.g. fracturing in rock or clay)). This is broadly referred as media degradation in the present study.

This modelling study examines the effects of media degradation on diffusion dominant solute transport in fractured media that are typical of deep geological environment. In particular, reactive solute transport through fractured media is studied using a 2-D model, that considers advection and diffusion, to explore the coupled effects of kinetic and equilibrium chemical processes, while the effects of degradation is studied using a pore network model that considers the media diffusivity and network changes.

Model results are presented to demonstrate the use of a 3D pore-network model, using a novel architecture, to calculate macroscopic properties of the medium such as diffusivity, subject to pore space changes as the media degrade. Results from a reactive transport model of a representative geological waste disposal package are also presented to demonstrate the effect of media property change on the solute migration behaviour, illustrating the complex interplay between kinetic biogeochemical processes and diffusion dominant transport.

The initial modelling results demonstrate the feasibility of a coupled modelling approach (using pore-network model and reactive transport model) to examine the long term behaviour of deep geological repositories with media property change under complex geochemical conditions.

INTRODUCTION

Diffusion phenomena in low-permeability rock (or clay) are of great importance in the study of containment performance of engineered barriers for deep geological radioactive waste repository. A typical deep repository is likely to be hundreds of metres below ground where the groundwater flow is very slow. At such condition radionuclide transport is mostly dominated by diffusion and sorption, with the additional effects due to the diffusive transport of reactive species that also leads to chemical zonation around waste packages which could provide additional containment of radionuclides.

Over the long 'operational' lifespan of a deep repository, the system is likely to be subjected to a variety of thermo-hydro-chemo-mechanical (THCM) effects that could reduce the integrity of the barrier system over time (e.g. fracturing, corrosion, mineral dissolution etc). It is important that these effects (referred generally as degradation) are taken into account when assessing the long-term performance of the repository. Numerical models of groundwater flow, solute transport and chemical processes offer a viable and cost effective means to study the long term evolution of repository condition, and aid understanding of the behaviour and mobility of the contaminants.

This work aims to demonstrate the feasibility of a coupled modelling approach to examine the long term behaviour of deep geological repositories with media property change and complex geochemical processes. This includes firstly using a microstructure-informed pore network model to study the effect of media property change (e.g. degradation) to provide a mechanistic understanding of macroscopic parameters on transport properties such as diffusive coefficient and porosity. The derived macroscopic transport parameters can then be fed into a reactive transport code GRM (Gerneralised Repository Model) [1] to model the effects of media degradation under the influences of hydrogeological (diffusion dominant) and microbially mediated chemical effects in geological systems with low groundwater flows for deep geological disposal systems.

MICROSTRUCTURE-INFORMED MODELLING

Modelling Diffusion with Discrete Networks

A novel architecture has recently been proposed for the construction of microstructure-informed 3D pore-network models (PNM) to study mass transport through porous media [1]. These models conceptualise the material pore space with a set of pores some of which connected by throats to reflect material-specific geometric and topological properties determined experimentally, e.g. by X-ray computed tomography. The novel architecture considers a specific tessellation of space consisting of truncated octahedrons that seems to offer a regular and physically realistic representation of a volume containing pores [1]. This regularization of the pore space can be considered as a homogenisation process within a certain length scale, i.e. the cell size corresponds to the average distance between pores in a particular porous medium. A discrete PNM can then be derived from a group of cellular tessellations consisting of pores (of different sizes and at the centres of the cells) that are connected to the neighbouring cells by throats of various sizes (including zero size). These throats can be considered as conduits for mass transport under a prescribed driving force, e.g. pressure gradient for flow advection or concentration gradient for diffusion. One major benefit of the novel architecture is that it allows a higher pore coordination of up to 14, as opposed to previously used models that were based on cubic lattices that only allow a maximum pore coordination of six [3, 4]. The importance of a higher pore coordination representation in the PNM has been revealed by experimental investigations, e.g. [5, 6], which showed substantial fractions of pores were in fact coordinated by more than six throats. This could limit an effective representation of transport pathways, both locally and globally. An additional benefit of the novel architecture is that it allows construction of networks with a wider set of pore coordination spectra (i.e. fractions of pores coordinated by different number of throats) that conforms to the same average coordination number. This is particularly useful for fine tuning of the discrete model, such as to fit a particular experimental data. Another major potential use of the discrete PNM is that they allow for expedient calculations of macroscopic properties of the medium, e.g. permeability or diffusivity, that consider pore space changes under the effects of any conceivable mechanism.

The model has been previously used for exploring the link between micro-structural pore space data and macroscopic (engineering scale) permeability in cements [7, 8] and limestone [1], including the evolution of permeability with mechanical damage such as micro-cracking. For these systems, the available micro-structural data included both pore size distribution and pore throat size distribution together with connectivity parameters. Such set of data can define completely the model. However, for systems with much tighter pore spaces the current experimental techniques do not appear to allow resolution of sufficient number of throat sizes (if at all) and consequently information on pore coordination statistics/spectra are not available. This work considers bentonite for which the extraction of throat size distribution and pore coordination from experiments is impractical. Within the PNM framework, this work firstly demonstrates how the novel architecture can be used with a practical method to relate throat sizes to their neighbouring pores. Secondly, the study also presents a preliminary application of the model to examine diffusion within porous medium, particularly the effect of porosity on macroscopic diffusivity. With the use of a simple throat size variation relationship, the model demonstrates an analysis on the effects of non-mechanical pore space changes on macroscopic diffusivity. Illustrative scenarios considered include 'enlargement' of throats (e.g. due to corrosion processes) and 'shrinkage' of throats (e.g. due to precipitation, microbial processes such as bacterial invasion). For illustration purposes, throat size changes in both cases are assumed to be dependent on the concentration of

a solute species (or agent). The overall aim of this study is to show how microstructure- and mechanism-informed modelling can be used to examine macroscopic property change and derive evolution laws of a porous media which may be useful in supporting engineering-scale transport modelling such as that dominated by diffusion process and associated with media property changes over an extended period.

A brief outline of the model basis is given below. Fig. 1 shows: (a) a unit cell of the regular tessellation of space together with the associated pore and all possible throats; and (b) the discrete architecture for constructing a pore-network model using particular microstructure data. The final model consists of two types of bonds: six in the principal lattice directions (brown) and eight in the octahedral directions (turquoise). For a unit cell with length of the principal bonds L_p, the length of octahedral bonds is $L_o = L_p \sqrt{3} / 2$ and the volume of the unit cell is $V_c = L_p^3 / 2$.

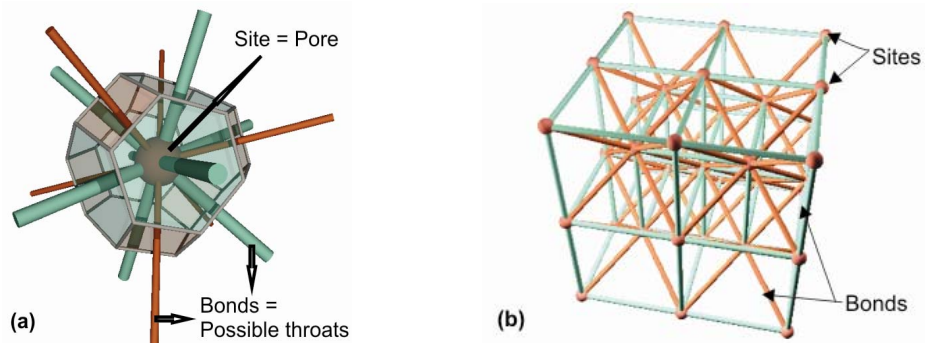

Fig. 1. (a) Unit cell of space tessellation showing associated pore at cell centre (lattice site) and all possible adjacent throats (lattice bonds); (b) Fragment of the discrete lattice architecture for construction of pore network with known microstructure properties.

Pore Size Distribution

Using this architecture the PNM construction starts with the distribution of pore sizes at the lattice sites according to an experimental pore size distribution. In this work recently reported results for bentonite is used, where hydrated bentonite systems have been cryogenically stabilised and analysed with a number of experimental techniques to resolve pore size distributions [10]. Of particular interest is the results of the high pressure frozen samples that provide high fidelity data of the clay pore space under hydro-geological conditions. The particular data used in this work is the 3D pore size distributions obtained for such samples with focused ion beam (FIB) nano-tomography which were presented as cumulative pore volume versus pore radius (Fig. 8 in [9]). The total porosity of the sample was $\theta = 0.68$. For the construction of PNM this information is converted into cumulative probability function of pore sizes, $F(r)$, using standard statistical technique, see e.g. [10]. The numerically derived $F(r)$ is shown in Fig. 2 with data points used shown as circular marks. In principle, this can be used directly to assign pore sizes using a generator of uniformly distributed random numbers $0 \le p < 1$; such that for a given random number p the pore size will be $r = F^{-1}(p)$. For the particular experimental data considered it was found that $F(r)$ can be fitted by the simple function:

$$F(r) = \frac{1}{1 + \left(\frac{r_0}{r} \right)^n} \qquad \text{(Eq. 1)}$$

where r_0 is the centre and n the shape of the distribution. Hence, for a given uniformly distributed random number p, the resolved pore size is:

$$r = r_0 \left(\frac{p}{1-p} \right)^{\frac{1}{n}} \qquad \text{(Eq. 2)}$$

The continuous function $F(r)$ (shown as solid curve) can be seen to provide an excellent fit to the experimental data (Fig. 2). These parameters and Eq. 2 have been used to distribute pore sizes randomly at the lattice sites, such that each complete distribution provides a particular realisation of the pore space.

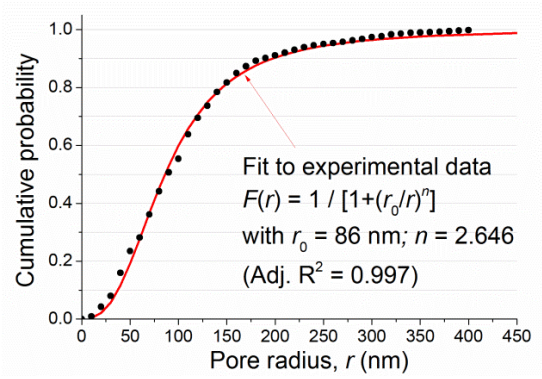

Fig. 2. Cumulative probability distribution of pore sizes in bentonite from data reported in [9]. Also showing the equation of a curve fit (to data) and the corresponding parameters.

Pore Throat Size Distribution and Connectivity

Since no information on throat sizes is available, the total volume of the distributed pores and a prescribed porosity of the medium, θ, define the length scale of the model, i.e. L_p defined above. Assuming pores of spherical shape with randomly assigned radii, the model length scale is found to be [2]:

$$L_p = \frac{8\pi}{3\theta N_c} \sum_{i=1}^{N_c} r_i^3 \qquad \text{(Eq. 3)}$$

where N_c is the number of cells in the model. For mass transport problems, this requires an assignment of links (throats) between neighbouring pores. This can be viewed as assignment of local diffusivity values or alternatively assignment of throat radii assuming cylindrically shaped throats. In the absence of throat size data and connectivity information, the throat radii need to be determined on the basis of available geometrical data, such as the radii of the two adjacent pores and the distance between them. One such possible approach is to study the relation between the prescribed porosity θ, and calculated macroscopic (effective) diffusivity, D, and compare this to the well-known scaling law $D/D_0 = \theta^{4/3}$, where D_0 is the diffusivity of species in an unconfined fluid region [11]. For the numerical experiments in this work we have considered a neutral U(VI) complex, $Ca_2\text{-}UO_2(CO_3)_3^0$. Experimental diffusivity of this complex in clay has been reported recently [12]. For illustration purpose, this diffusivity is used in the current model although more precise diffusivity value of the compound should ideally be considered. The estimated molecular size of such species is $R_s = 0.524$ nm. Using the Stokes-Einstein equation, e.g. [13], the molecular diffusivity of this complex in water (viscosity $\mu = 8.94\times10^{-4}$ Pa.s and at room temperature) can be determined $D_0 = 4.66\times10^{-10}$ m^2/s. For a given throat radius (R_t,), it is possible to determine its diffusivity value using $D_t = \alpha D_0$, where α is a steric hindrance factor accounting for the interaction between solute (solvent) and throat walls given by [14]:

$$\alpha = \left(1 - \frac{R_s}{R_t} \right)^4 \qquad \text{(Eq. 4)}$$

Hence, the description of the model would be completed once throat radii are determined. The steric effect will be small or negligible for large throats, and will increase for throats approaching the size of the diffusing solvent molecules. Note, that Eq. 4 requires $R_s < R_t$, otherwise the solvent molecules pass through the throat. This means that for the proposed architecture and approach, the pore connectivity will be influenced solely by the size of the solvent molecules. Although this topic will not be discussed in the work it is worth mentioning the following. For a given pore size distribution and selected methodology for calculating throat sizes, this means that the pore coordination spectrum would be dependent on the size of the diffusing solvent molecules, i.e. from low average coordination for large solvent molecules (down to 0 for fully impermeable for very large solvents) to high average coordination for small solvent molecules (up to 14 for fully permeable for very small molecules).

Results presented below are for a PNM of size $10L_p \times 10L_p \times 20L_p$ in a *X, Y, Z* coordinate system. The resulting model consists of 3,540 pores and 22,000 possible throats. The pores on faces $X = 0$, $X = 10L_p$, $Y = 0$, and $Y = 10L_p$, have been prescribed a zero-flux boundary condition. The pores on faces $Z = 0$ and $Z = 20L_p$, have been prescribed concentrations $C_0 = 1$ and $C_1 = 0$, respectively, as boundary conditions for the diffusion process. This boundary value problem corresponds to an experiment with a column of length $L_e = 20L_p$, and cross-sectional area $A_e = 100L_p^2$, where a concentration difference, $\Delta C = 1$, is applied at the column ends with impermeable side walls. This study considers only steady-state solutions as the main interest is on deriving macroscopic diffusivity of the synthetic pore system, although transient solutions can be readily studied using the current model which will be reported in the future. The above system is solved using a standard FEA program with 1D solid diffusion elements representing throats (lattice bonds). For the steady state case, the system diffusivity D is obtained from the total flux, J, calculated at equilibrium over any of the column ends, i.e. the sum of fluxes through pores at $Z = 0$ or $Z = 20L_p$. For a given concentration difference and assuming Fick's law, $D = J \times L_e / A_e$.

In the absence of throat size and pore connectivity data, several scenarios have been considered for determining throat size, using models over a prescribed porosity range $0.2 \leq \theta \leq 0.8$. Note that the cumulative pore size distribution remains the same for these cases, Eq. 1. For each of the porosity cases, 30 calculations are performed using random distributions of pore sizes. Some of the possibilities, suggested in the past, include calculations of throat radii, R_t, as functions of the radii of the two neighbouring pores, r_1 and r_2, only. Examples are harmonic means, $2/R_t = 1/r_1 + 1/r_2$, and weighted geometric means, $R_t = r_1^{\lambda} \times r_2^{1-\lambda}$, where $0 \leq \lambda \leq 1$ is a weighting factor to relate the throat size to the connecting pores. While these suggestions can be supported by heuristic geometrical arguments, it is found that they yield system diffusivity that scales with the porosity closely to the power of 2/3, for all values of λ. and random distributions considered. Although these results are not presented here, this observation suggests that $D/D_0 \sim \theta^{2/3}$ when throat sizes relate only to the sizes of the connecting pores. Such approach implies the physical distance between the pores is intrinsically related to the throat size, and thus the local diffusivity. This approach is reciprocal to the calculation of pore sizes from known throat sizes adjacent to the pore used in [14]. Based on a simple geometric construct the following expression for throat size is proposed:

$$R_t = \frac{r_1 r_2}{2}\left(\frac{1}{\sqrt{d^2 + r_1^2}} + \frac{1}{\sqrt{d^2 + r_2^2}}\right) \qquad \text{(Eq. 5)}$$

where r_1 and r_2 are the radii of the pores connected by the throat, and d is the physical distance between them, i.e. $d = L_p$, or $d = L_o$, depending on the type of the throat. With the model constructed using Eq. 5 the scaling law, $D/D_0 \sim \theta^{4/3}$, is reproduced with high accuracy. This is illustrated in Fig. 3, where the parameter $y = -\log(D/D_0)$ is plotted against $x = -\log(\theta)$ for three selected random distributions of pore sizes. These correspond to the lower bound, the median and the upper bound results out of the 30 different pore size distributions simulated.

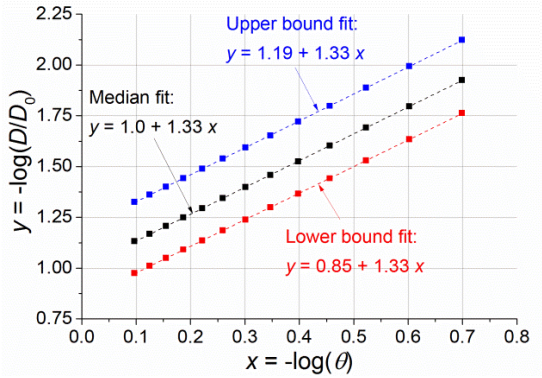

Fig. 3. Dependence of model diffusivity on porosity. Results from three random distributions of pore sizes are given together with the corresponding linear fits to simulated data.

It is clear that the scaling law is reproduced irrespective of the random distribution of pore sizes. The differences observed for different distributions are in the constant term, which is not zero as the scaling law $D/D_0 = \theta^{4/3}$ states. The reason for this is that the model also likely captures network tortuosity effects and possibly local steric hindrance effects, suggesting that the results provide an apparent diffusivity, D_a, of the medium. The variability between different random distributions may be attributed to the effect of the 'finite' model size, i.e. the model domain/size used may be smaller to what would be the 'representative' volume for this medium. The variability is expected to be reduced by larger models and should diminish when the material representative volume is covered. This effect should be studied in more details in future studies. The results are compared with available experimental data [15], where the apparent diffusion coefficient for bentonite samples with porosities θ = 0.62 to 0.64, is found in the range $D_a = 1.16 \times 10^{-12}$ m^2/s to 2.30×10^{-12} m^2/s. Our solutions for D/D_0 for the porosities within this range vary between 0.008 and 0.05, providing an apparent diffusion coefficient in the range $D_a = 4.2 \times 10^{-12}$ to 2.3×10^{-11} m^2/s. The results differ by up to an order of magnitude. In principle, the model can be tuned further by scaling the throat sizes given by Eq. 5 to better match the experimental data. However, the experimental values are likely to include sorption effects that are not currently accounted/included in the model. This makes the additional tuning less essential at this stage. The main conclusion from the present study is that the PNM can produce realistic apparent diffusion coefficients that are consistent with experimental data. This strongly supports its use for future studies of pore-space evolution and effects on the diffusivity of porous medium.

To illustrate the effects of corrosion-driven 'enlargement' and microbial- (such as bacterial-) driven 'shrinkage' of throats, the rate of change of a throat radius, R_t, is assumed as $dR_t = R_t \, \kappa \, d\chi$, where $d\chi$ is the change of local concentration of the agent and κ is a rate constant. This provides a simple mathematical framework to represent/treat both processes, noting that $\kappa < 0$ corresponds to cases of microbial effects, while $\kappa > 0$ corresponds to cases of corrosion effects, and $\kappa = 0$ corresponds to unchanged pore space. Integration of the rate equation gives:

$$R_t(\chi) = R_t(0)\exp(\kappa\chi) \qquad \text{(Eq. 6)}$$

where $R_t(0)$ is the throat radius at agent concentration $\chi = 0$, i.e. the originally calculated radius, and $R_t(\chi)$ is the radius at concentration χ. Two cases are considered here for the distribution of the agent (as opposed to solvent) in the pore space. In the first case the agent is driven by a concentration difference with the boundary conditions $\chi = 1$ at $Z = 0$ and $\chi = 0$ at $Z = 20L_p$, such that the concentrations of both the solvent and agent are decreasing along the positive Z direction. This is referred to as the 'forward invasion'. In the second case the agent is driven by a concentration difference with the boundary conditions $\chi = 0$ at $Z = 0$ and $\chi = 1$ at $Z = 20L_p$, such that while the solute concentration increases along the positive Z-direction, the agent concentration decreases along the same direction. This is referred to as the 'backward invasion'. To simplify the solution in

the current work, the local diffusivity of the agent is assumed to be the same as the local diffusivity of the solvent. This assumption is not unrealistic for corrosive agents, but could be an oversimplification with more complex microbial processes, where local diffusivities may be small due to large size of the agent molecules that may not be able to pass through a large fraction of the smaller throats. These effects would be of interest to study in the future. In the present study, this simplification is adopted merely to illustrate in practice diffusion process could be influenced by various processes such as dissolution and/or precipitation which could be related to solvent concentrations (or any other parameters deemed appropriate for the process considered) as a basis for pore space changes. Here, the size of a given throat is calculated from Eq. 6, where $\chi = C$ for parallel invasion and $\chi = 1 - C$ for opposite invasion, where C is the solvent concentration within the throat region. This non-linear problem is solved with the same standard FEA program as above.

For each porosity case, this study involves model runs using 30 different random distributions of pore sizes for calculating the macroscopic diffusivities for pore space changes over the rate interval $-1.5 \leq \kappa \leq 1.5$. The dependence of macroscopic diffusivity, given by $\log[D(\kappa)/D(\kappa=0)]$, on the rate is shown in Fig. 4 for one model realisation with both parallel and opposite agent invasions. Note, that $D(\kappa=0) = D(0)$ corresponds to the solution for the system diffusivity without pore space changes, which is identical to the solution with zero concentration of agent given above. It is clear from the results that for the current approach the steady-state diffusion coefficient depends only on the rate of the pore space changes. The results show the direction of invasion has no effect on the value of the steady-state diffusion coefficient. However, this does not mean that the spatial variation (profile) of solvent concentration is the same for both 'directional' cases. For instance, Fig. 5 shows the concentration profiles of the solvent for the same model realisation as in Fig. 4. The results are for the case of corrosion with rate of throat expansion $\kappa=1$ with corrosive agent diffusion for the forward and backward invasion cases. The distance is measured from $Z = 0$, where $C = 1$, and scaled by the model physical length, L_e. The concentration at a given distance Z is calculated as the average value over the pores over an interval at the distance. The profile without pore space changing agent is also shown for comparison - it is approximately linear as expected.

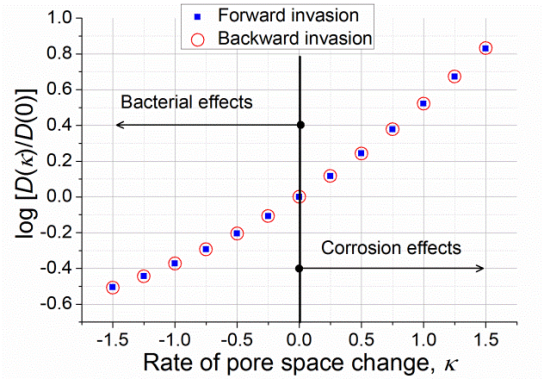

Fig. 4. Change of macroscopic diffusion coefficient with pore space changes. Corrosion effects are exemplified by positive rates; Bacterial effects are exemplified by negative rates. Results for both forward and backward invasion of these agents are shown.

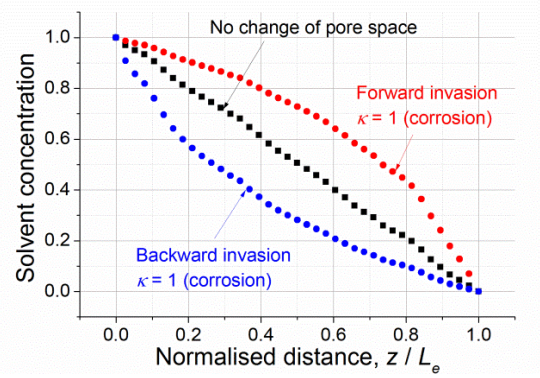

Fig. 5. Steady-state concentration profiles of solvent, U(VI), as predicted by the model with pore space changes due to corrosive agent diffusing in parallel with (forward) and opposite to (backward) solvent diffusion. Profile with no pore space changes shown for comparison.

The diffusivity-rate relation shown in Fig. 4 has been found to be the same for all 30 model realisations. This is not shown in the figure as all solution points will overlap, but indicates that the particular distribution of pore sizes does not affect the changes in the steady-state diffusion coefficient. The effects of the pore size distribution and invasion direction are expected to be only apparent in the transient cases. The pore space change given by Eq. 6 is exponential. If all throats are expanding or contracting with linearly changing rate, the $\log[D(\kappa)/D(\kappa=0)]$ should be a linear function of this rate. The non-linear dependence shown in Fig. 4 indicates strong effect of the changing network connectivity. For positive rate exemplifying corrosion, throats with originally very small radii (hence diffusivity) are expanding and creating shorter pathways for diffusion within the global network. Inversely, for negative rates exemplifying bacterial effects, throats with originally larger radii (hence diffusivity) are contracting and reducing exiting pathways for diffusion. In fact the non-linear effect of connectivity changes is more pronounced for the bacterial effects. Further research is needed for better characterisation of the connectivity effects, e.g. by decoupling the diffusion of agents from the diffusion of solvent as mentioned above.

ILLUSTRATIVE MODEL OF A GEOLOGICAL WASTE DISPOSAL PACKAGE

An illustrative two-dimensional reactive transport model has been previously developed [18] to examine the coupled effects of a geological waste disposal package between;

- diffusion dominant transport;
- kinetic controlled microbial processes; and
- equilibrium chemical speciation, mineral and radionuclide dissolution and precipitation.

The present study investigates further the effect of medium change, such as degradation, on solute transport for such a waste package. The model represents a generic case relevant to geological disposal of TRU/ILW where a disposal waste package containing contaminants (uranium) and other multivalent reactive species (iron, sulphate, nitrate) are enclosed in a highly impermeable but reactive medium where diffusion is the main transport mechanism. Iron is in the form of Fe(II) and represents corrosion products present in waste and containers used. The effect of a sealed waste package container (to physically isolate the waste) is not considered in this scenario. The present model therefore examines the effects that may develop after any such containment is breached. The model examines how the evolving chemical conditions of the repository and diffusive properties of the waste and enclosing medium may affect the containment/mobility of the uranium, when the effect of medium degradation is also considered. The enclosing medium has neutral pH and may represent a low permeability enclosing medium, such as clay or backfill. Along a boundary of the model is an advective transport pathway, which can be considered to represent features such as fractures present in the

containment medium. Groundwater that saturates the waste package contains organic matter, and it is assumed that the containment medium of the disposal facility and other engineering maintain reducing conditions external to the waste package. These strongly reducing conditions are represented by the partial pressure of hydrogen (0.99 atm H_2) in the model.

The model is configured in a 2-dimensional array of 20 x 20 cells (Fig. 6) where a single row of 20 cells represents an advective region and 19 adjacent rows of 20 cells represent the diffusive zone (no advective flow) including an area of waste source with kinetic release over time. The model considers an area of 5m by 0.48m. The advective row has a width of 0.1m while the remaining 19 rows representing the diffusive regions are of 0.02m width.

The main diffusive region of interest is within the 19 rows over a width of 0.38m (38cm), including the waste region and enclosing medium. Note that the width (or breadth) of the diffusive region is exaggerated in the figures. A groundwater flow rates of 10 ml/day was considered in the advective region.

Moore and Shackelford [17] have undertaken a literature review on the liquid-phase diffusion of uranium through natural soils and rocks including compacted soils used as engineered barriers (e.g. compacted bentonites). The study [17] noted the diffusion coefficient in a number of compacted bentonite could vary over a wide range (e.g. $4.3\text{x}10^{-14} \leq D \leq 1.8\text{x}10^{-10}$ m^2/s), while D tends to increase semilog linearly with increasing porosity, and also could be potentially affected by chemical speciation. In the present study, an effective diffusion coefficient of $D = 2.8 \times 10^{-10}$ m^2/s is used, which although significantly higher than the values of 1.0×10^{-11} m^2/s previously used, this falls within the diffusivity range typical of compacted bentonites [17].

The waste region (shaded red/purple in Fig. 6) contains uranium at a concentration of 1.0×10^{-3} mol/l of pore fluid. The presence of Fe(II) corrosion products in the form of $FeCO_3$ are considered in the waste. The model also considers that reactive chemical species nitrate and sulphate are present in the TRU/ILW waste in the two regions: region 1 (shaded purple) has concentration of 5.0×10^{-3} mol/l NO_3^- while region 2 (shaded red) has a lower concentration of 1.0×10^{-3} mol/l. The sulphate concentration in both regions is 1.0×10^{-3} mol/l. Chloride is also present in the waste at a concentration of 1.1×10^{-1} mol/l in region 1 or 1.5×10^{-1} mol/l in region 2 (to balance the nitrate) to provide charge balance to compensate for the additional nitrate in region 1. Chloride is not reactive in the model.

The enclosing diffusive medium (clay) is represented by the calcium and iron containing carbonates (calcite, siderite), which is defined by a partial pressure of carbon dioxide (1.45×10^{-2} atm CO_2) that buffers pH to near neutral conditions. Sulphate minerals present in the clay (gypsum, celesite) similarly control the sulphate concentration in groundwater that saturates the clay. The groundwater that saturates the waste and enclosing clay also contains dissolved organic matter, which in the GRM is represented by an acetate concentration of 9.2×10^{-5} mol/l.

GRM was used to simulate a period of 100 years of reaction and diffusion. GRM is a computer code [1], originally developed by the Research and Technology department of BNFL (now the National Nuclear Laboratory), to model the long term chemical evolution of both the near surface and deep disposal facilities. Reference [1] gives more details of the full suite of microbiological processes, chemical speciation, mineral reaction, including radionuclide solubility and sorption. Reference [19] documents details of a wide range of test cases which have been designed to test the extensive capabilities of the GRM program.

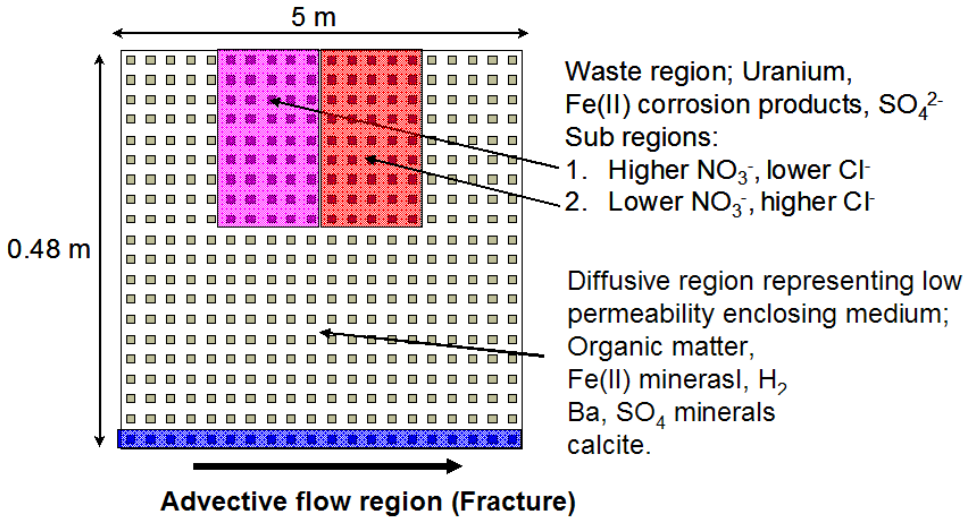

Fig. 6. Schematic illustration of the GRM reactive transport (advection and diffusion) application model [18].

REACTIVE TRANSPORT MODELLING RESULTS

Using the GRM model the above geological waste disposal package is considered to examine the combined effect of kinetic biogeochemical processes and diffusive dominant transport for a new basecase medium scenario with a higher effective diffusion coefficient $D = 2.8 \times 10^{-10}$ m^2/s (compared to 1.0×10^{-11} m^2/s studied in [18]) to derived from the above PRM analysis, under the influence of media degradation and fracture.

Base Case

With the initial conditions described above, the system representing a TRU/ILW waste package (with medium properties $D = 2.8 \times 10^{-10}$ m^2/s and θ=0.68) was modelled for a period of 100 years. Fig. 7 presents summary outputs at the end of the simulation period. Fig. 7a illustrates the diffusive behaviour of chloride, which is both non reactive and non-sorbing. Chloride presents in the waste region (purple region in the figure) diffuses away from the source, such that after 100 years the peak concentration reduces to below 3.56×10^{-2} mol/l (i.e. about 0.78 of the initial maximum concentration in the waste region). The remaining figures illustrate the biogeochemical reactions occurring mediated by microbial processes. The presence of nitrate in the waste results in its rapid reaction by denitrifying bacteria, which utilise organic carbon, H_2 and Fe(II) as electron donors. The oxidation of Fe(II) corrosion products results in the formation of $Fe(OH)_3$. (Fig. 7b), with the amount of $Fe(OH)_3$ formed proportional to the nitrate content of the waste.

The redox potential (Eh) determined by the kinetic routine is illustrated in Fig. 7c, which shows that the oxidation of Fe(II) to Fe(III) in the waste to maintain a higher Eh at around -0.1 volts. It is observed that this oxidised zone extends into the adjacent clay by diffusion of species and the precipitation of $Fe(OH)_3$, (Fig. 7b). In the majority of the clay zone sulphate reduction occurs due to the dissolved organic matter input from groundwater passing through the advective region that diffuses through the clay zone. Hydrogen present also acts as an electron donor for sulphate reduction. More strongly reducing conditions are established at the inlet of the advective fracture, where sulphate becomes totally reduced by the inflowing organic carbon. The microbial biomass that results from these main reactions of the electron acceptors and donors present is illustrated in Fig. 7d. Most microbial activity is seen to occur in the waste region and at the interface with the clay zone. A further region of microbial activity occurs near the inlet of the advective region.

The resulting diffusive and chemical effect on uranium is illustrated in Fig. 7e and Fig. 7f. In the waste region uranium is in the U(VI) oxidation state and has high solubility. Aqueous uranium becomes mobile and readily

diffuses from the waste. Under the sulphate reducing conditions established in the clay, uranium precipitates as UO_2(am) and thus the concentration of dissolved uranium falls significantly compared to that of the non-reactive chloride species (Fig. 7a). The migration of uranium from the waste region is affected to a small extent by the different nitrate contents of the waste in region 1 and region 2 (Fig. 6). Uranium is also precipitated in the advective zone, where the very strongly reducing conditions are developed. The uranium concentration exiting the advective zone is 5.95×10^{-6} mol/l and is of similar magnitude to the concentration level in the waste region. With a higher diffusion coefficient (compared to [18].), the concentration gradient of uranium across the diffusion zone is reduced.

The effects of media degradation (e.g. fracture and media porosity changes) on solute transport relevant to the long term prediction of containment performance are illustrated below. This highlights the need for a mechanistic understanding and quantification of the macroscopic parameters and their evolution. The later section "Microstructure-Informed Modelling" outlines an ongoing work on microstructure-informed modelling approaches and concepts, and highlights its potential in supporting solute transport modelling that taking account the effects of media degradation.

Effect of Medium Diffusive Property Changes

The effect of effective diffusion coefficient change due to porosity change of the enclosing media is examined by making use of the well-known MQ model [20], $D = D_o \theta^{\frac{4}{3}}$, with a constant solute's diffusion coefficient (D_o). Over the long time scale typical of geological disposal applications, the porosity of the enclosing media may change over time as the pore spaces evolve under the influence of various effects such as degradation due to chemical effects and corrosion. Modelled results are presented below to illustrate the effects of reduced (effective) diffusion coefficient of 2.2×10^{-10} m^2/s due to a decrease in porosity to 0.8, such as due to precipitation. (Compares to Base Case with $D = 5.8 \times 10^{-12}$ m^2/s and $\theta = 0.68$).

Similar to the Baseline case, most of the biomass occurs in the waste region and adjacent area (Fig. 8a), with decrease in porosity leading to a slight drop in biomass production in these areas. The biomass area adjacent to the waste is also seen to spread over a slightly smaller area at lower porosity due to reduced diffusion rate. Biomass also occurs near the fracture inlet region where a strongly reducing condition is established. The effect of diffusivity (and porosity) change is negligible in this region as this is dominated by the advective flow.

As Fe(II) in the waste oxidises to Fe(III), this oxidised zone is diffused into the adjacent clay with the precipitation of $Fe(OH)_3$ (Fig. 8b). The change in diffusivity seems to have little effect on the level of $Fe(OH)_3$ within the waste zone, but resulting in a very slight drop over the adjacent (and less diffused) region.

Fig. 8c to Fig. 8d show the effect of porosity change on uranium under the combined influence of diffusive and chemical actions. It can be seen that a lower porosity case shows a higher peak aqueous uranium concentration within the waste region with a lower concentration in the adjacent clay due to the reduced diffusion rate, Fig. 8c. Similar effect can be seen on uranium precipitation. The effect is more pronounced in the waste region, but is less significant in the adjacent clay region for the lower porosity case.

The modelled results illustrate the complexity of solute transport behaviour that could occur in a waste disposal facility, due to the interplay between kinetic biogeochemical processes and diffusion due to medium property changes.

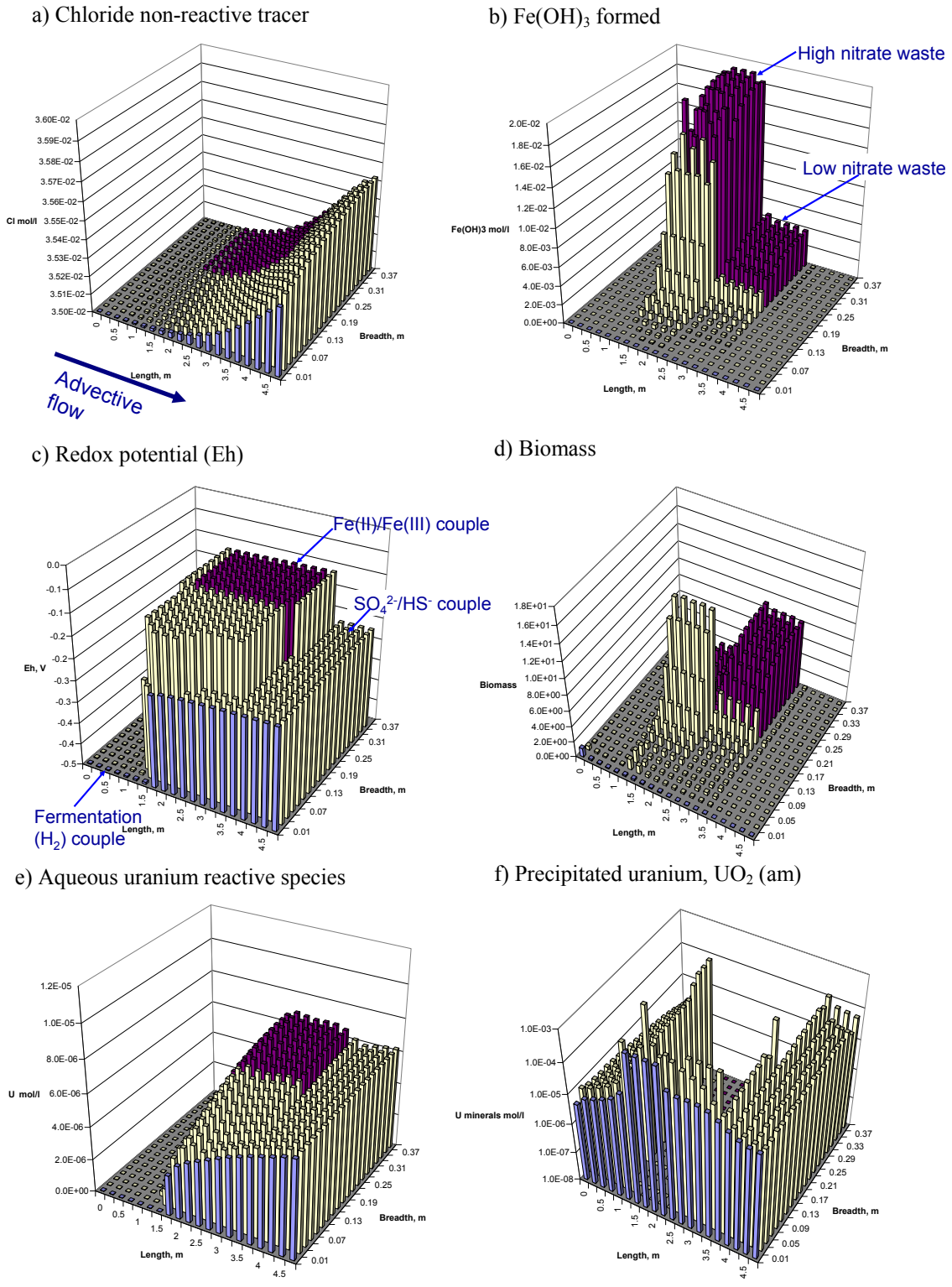

Fig. 7. Base Case model results of an illustrative waste package in a geological repository after 100 years.

a) Biomass

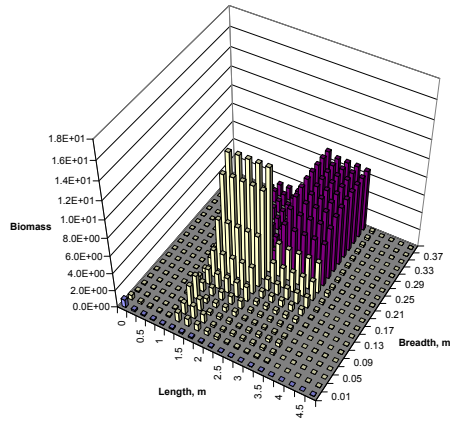

b) $Fe(OH)_3$ formed

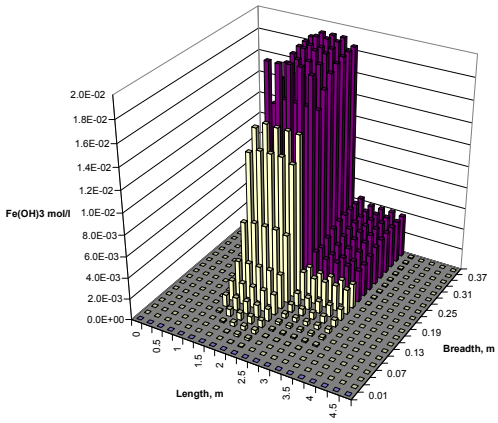

c) Aqueous uranium reactive species

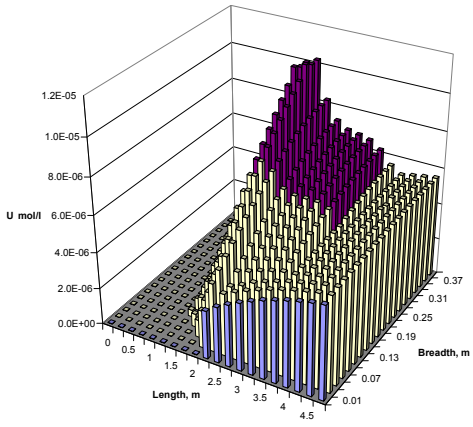

d) Precipitated uranium, UO_2 (am)

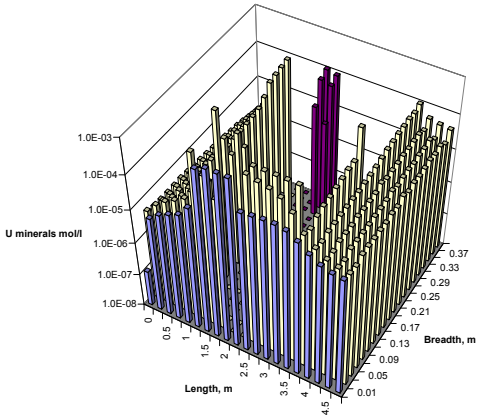

Fig. 8. Model results after 100 years for a lower effective diffusion coefficient D= 2.2 $\times 10^{-10}$ m^2/s, due to a 17.6% porosity decrease to 0.56.

CONCLUSIONS

In this work a pore network model using a novel architecture has been successfully used for predicting diffusivity of porous media with minimum amount of experimental data, using only the cumulative distribution of pore sizes. The approach provides a potential means to model media with very tight pore spaces when information on pore coordination statistics/spectra is not available (due to the lack experimental technique to resolute sufficient number of throat sizes). This applies to many low permeability media such as the bentonite considered here, where the sizes of diffusion pathways (pore throats) cannot be adequately resolved with most of the existing experimental techniques. Specifically the new model has reproduced accurately the scaling relation between the macroscopic (apparent) diffusion coefficient and porosity of the medium, and predicts the apparent diffusivity of U(VI) in bentonite that agrees well with experimentally measured values. This strongly suggests the modelling approach has captured the essential correlation between micro-structural features and macroscopic transport properties of the medium. The proposed model is therefore likely to be appropriate for studies of diffusivity evolution of porous medium involving pore space changes. Some simple calculations have been presented to illustrate model applications using a simplified representation of corrosion (pore space enlarging) and bacterial (pore space reducing) effects. The initial results seem promising and realistic. Although results reported above are mainly relevant to steady-state diffusive condition, the model can be readily extended to study transient situations.

Model results from a reactive transport model of a representative geological waste disposal package are also presented to demonstrate the effect of media property change on the solute migration behaviour. This illustrates the complex interplay between kinetic biogeochemical processes and diffusion dominant transport.

The initial model results are encouraging. This illustrates the feasibility of a coupled modelling approach, using pore-network model and reactive transport model, to examine the long term behaviour of deep geological repositories with media property change under complex geochemical conditions.

REFERENCES

1. S. Kwong. (2009a). Program User's Guide for the code GRM, Version 6.1. NNL Report.
2. A.P. Jivkov, C. Hollis, F. Etiese and P.J. Withers (2012). "A novel architecture for pore network modelling with applications to permeability of porous media ". J. Hydrol., accepted.
3. G.P. Matthews and M.C. Spearing (1992). "Measurement and modelling of diffusion, porosity and other pore level characteristics of sandstone". Marine Petrol. Geol. Vol 9, pp. 146-154.
4. P.C. Reeves and M.A. Celia (1996). "A functional relationship between capillary pressure, saturation and interfacial area as revealed by a pore-scale network model". Water Resour. Res. Vol 32, pp. 2345-2358.
5. R.I. Al-Raoush and C.S. Wilson (2005). "Extraction of physically realistic pore network properties from three-dimensional synchrotron X-ray microtomography images of unconsolidated porous media images". J. Hydrol. Vol 300, pp. 44-64.
6. H. Dong and M.J. Blunt (2009). "Pore-network extraction from micro-computerized-tomography images". Phys. Rev. E Vol 80, p. 036307.
7. A.P. Jivkov and J.E. Olele (2012). "Novel lattice models for porous media". In "Scientific Basis for Nuclear Waste Management XXXV", R.M. Carranza, G.S. Duffo and R.B. Rebak (Eds.), MRS Symp. Proc. Vol 1475, pp. 565-570, Cambridge University Press.
8. S. Kwong and A.P. Jivkov (2012). "Diffusion dominant solute transport modelling in fractured media under deep geological environment". In: Proc. WM2012 2012, Phoenix, US.

9. L. Holzer, B. Munch, M. Rizzi, R. Wepf, P. Marschall and T. Graule (2010). "3D-microstructure analysis of hydrated bentonite with cryo-stabilized pore-water". Appl. Clay Sci. Vol 47, pp. 330-342.

10. K. Meyer and P. Klobes (1999). "Comparison between different presentations of pore size distribution in porous materials". Fresenius J. Anal. Chem. Vol 363, pp. 174-178.

11. R.J. Millington (1959). “Gas diffusion in porous media”. Science Vol 130, pp. 100-102.

12. J. Bai, C-H. Liu and W.P. Ball (2009). “Study of sorption-retarded U(VI) diffusion in Hanford silt/clay material”. Environ. Sci. Technol. Vol 43, pp. 7706-7711.

13. M. Cappelezzo, C.A. Capellari, S.H. Pezzin and L.A.F. Coelho (2007). “Stokes-Einstein relation for pure simple fluids”. J. Chem. Phys. Vol 126, p. 224516.

14. L.M. Bryntesson (2002). “Pore network modelling of the behaviour of a solute in chromatography media: transient and steady-state diffusion properties”. J. Chrom. A Vol 945, pp. 103-115.

15. X.K. Wang, C.L. Chen, X. Zhou, X.L. Tan and W.P. Hu (2005). “Diffusion and sorption of U(VI) in compacted bentonite studied by a capillary method”. Radiochim. Acta Vol 93, pp. 273-278.

16. P. L. McCarty and F. E. Mosey. (1991). Modelling of Anaerobic Digestion Processes (A Discussion of Concepts), Water Sci. Technol. 24 No.8, pp.17-33.

17. S.M. Moore and C.D. Shackelford. (2011). "Uranium diffusion in soils and rocks", Proceedings Tailings and Mine Waste 2011, Vancouver.

18. S. Kwong and A.P. Jivkov. (2012) "Diffusion dominant solute transport modelling in fractured media under deep geological environment", Paper 12211, Proceedings of WM2012: The Waste Management Symposium 2012, Phoenix, US.

19. S. Kwong. (2009b). Program Verification Report for the code GRM, Version 6.1. NNL Report.

20. R.J. Millington and J. M. Quirk, "Permeability of porous solids". Trans. Faraday Soc. 57:1200-1207 (1961).